Electronic Supplementary Material (ESI) for Journal of Materials Chemistry C.
This journal is © The Royal Society of Chemistry 2022

1. General Methods:

1.1. Synthetic Methods

Unless otherwise noted, chemical reagents were purchased from commercial suppliers and used without further purification. 4,4′-ditertbutyl-2,2′-bipyridyl was purchased from Sigma Aldrich and used as received. $NiCl_2$.glyme was purchased from Strem and used as received. The metallophotoredox catalyst, $[Ir\{dF(CF_3)ppy\}_2(dtbpy)]PF_6$, was prepared in two steps from $IrCl_3$ *via* the method of Lowry *et al*. [1] The sp^3-sp^3 metallophotoredox coupling reactions [2] were performed in 25 ml reaction tubes (Sigma Aldrich, part no. Z515981. Irradiation was from two LED emitters (Mouser, part no. LZ1-10UB00-00U8, 405 nm peak output, 1050 mW radiant flux) mounted on anodised aluminium heatsinks (Mouser, part no. 984-ATSEU-077B-C6-R0) at opposite sides of the reaction tube at a distance of approximately 1 cm from the wall of the reaction tube. The LED and reactor assembly was cooled with a fan during operation. Nickel mediated decarboxylative alkyl-alkyl cross couplings of N- hydroxyphthalamide esters with organozinc reagents were performed *via* the method of Qin *et al*. [3] 4-(Pent-4-eneyloxy)-4′-cyanobiphenyl was prepared as reported previously. [4] 5-Cyclohexylpentan-1-ol was prepared *via* the method of Perez *et al.* in > 95 % yield using lithium aluminium hydride in THF. [5] 6-Cyclohexylhexan-1-ol was prepared according to Liu *et al*. [6] THF and dichloromethane were purchased from Fisher Scientific UK and were dried *via* passage over activated alumina. Diethyl ether was purchased from Fisher Scientific UK and dried over calcium hydride and distilled prior to use.

Reactions were monitored by thin layer chromatography (TLC) with DCM as the eluent. Silica coated aluminium TLC plates used were purchased from Merck (Kieselgel 60 F-254) and visualised using either UV light (254 nm and 365 nm), or by oxidation with either iodine or aqueous potassium permanganate solution. Yields refer to chromatographically (HPLC) and spectroscopically (^{1}H NMR, $^{13}C\{^1H\}$ NMR) homogenous material.

1.2. Characterisation Methods

1.2.1. Nuclear Magnetic Resonance (NMR)

NMR spectra were recorded on a JEOL ECS spectrometer operating at 400 MHz (^{1}H) or 100.5 MHz ($^{13}C\{^{1}H\}$) as solutions in $CDCl_3$.

1.2.2. Mass Spectrometry (MS)

Mass spectra were recorded on a Bruker compact time of flight mass spectrometer with both ESI and APCI sources, and we extend our gratitude to Mr. Karl Heaton of the University of York for obtaining MS data.

1.2.3 High Performance Liquid Chromatography (HPLC)

High-performance liquid chromatography was performed on a Shimadzu Prominence modular HPLC system comprising a LC-20A solvent pump, a DGU-$20A_5$ degasser, a SIL-20A autosampler, a CBM-20A communication bus, a CTO-20A column oven, and a SPO-20A dual wavelength UV-vis detector operating at wavelengths of 220 and 250 nm. Reverse-phase HPLC was performed using an Alltech bonded silica column with a 5 μm pore size, an internal diameter of 4.6 mm and a length of 250 mm, with neat dichloromethane used as the mobile phase. Chromatograms where only one peak was detected are quoted at >99.9% purity.

1.2.4. Polarised Optical Microscopy (POM)

Polarised optical microscopy was performed on a Zeiss Axioskop 40Pol microscope using a Mettler FP82HT hotstage controlled by a Mettler FP90 central processor. Photomicrographs were captured *via* an InfinityX-21 MP digital camera mounted atop the microscope.

1.2.5. Differential Scanning Calorimetry (DSC)

Differential scanning calorimetry was performed on a Mettler DSC822^e calibrated before use against indium and zinc standards under an atmosphere of dry nitrogen. DSC thermograms were processed in Matlab.

1.2.5. Small Angle X-ray Scattering (SAXS)

Small angle X-ray diffraction was performed using a Bruker D8 Discover equipped with a temperature controlled, bored graphite rod furnace, custom built at the University of York. The radiation used was copper Kα (λ = 0.154056 nm) from a 1 μS microfocus source. Diffraction patterns were recorded on a 2048x2048 pixel Bruker VANTEC 500 area detector set at a distance of 121 mm from the sample, allowing simultaneous collection of small angle and wide angle scattering data. Samples were filled into 0.9 mm OD glass capillary tubes and placed into the graphite rod furnace. Alignment of the sample was achieved with a pair of 1T magnets, with the field perpendicular to the incident X-ray beam. Diffraction patterns were collected as a function of temperature (controlled to a precision of +/- 0.1 °C). Two dimensional diffraction patterns were radially averaged (0.05 ° step size) to give one dimensional profiles of scattered intensity as a function of two theta. D-spacings were obtained by fitting the radially averaged data with a Gaussian, Lorentzian or Voigt function, as appropriate.

1.2.6. Computational Chemistry

Computational chemistry was performed using Gaussian G09 revision e01 on the York Advanced Research Computing Cluster (YARCC) at various levels of theory as described in the text. [7]

1.3. General Synthetic Protocols

1.3.1. General Mitsunobu Procedure:

An oven dried round bottom flask was charged with 4-hydroxy-4′-cyanobiphenyl (1 eqvl), PPh_3 (1.2 eqv) and - if solid - the alcohol (1 eqv). The flask was cooled to 0 °C with an ice bath under an internal atmosphere of dry nitrogen and the solids dissolved into anhydrous THF (20 ml). The reaction solution was cooled to 0 °C and DIAD (1.2 eqv) and added. The reaction was then monitored by TLC until complete consumption of the phenol and alcohol (typically < 4h). Celite (1 g per mmol of alcohol) was added, the suspension was then stirred for 5 minutes, and the solvent was removed *in vacuo*. The celite-loaded crude reaction mixture was purified by flash chromatography with a gradient of hexanes/DCM. The chromatographed material was redisolved into DCM and passed through a 0.2 µm syringe filter before removing the solvent *in vacuo* and recrystallizing from ethanol/THF mixtures.

1.3.2. General Esterification Procedure:

The liquid carboxylic acid (1.2 eqv) was added in one portion to a stirred suspension of 4-hydroxy-4′-cyanobiphenyl (1 eqv) EDAC (1.5 eqv) DMAP (catalytic) in DCM (5 ml per mmol). The reaction was monitored by the consumption of 4-hydroxy-4′-cyanobiphenyl (Rf_{DCM} ~ 0.3) and the formation of the product (Rf_{DCM} ~ 0.65) as evidenced by TLC. The solvent was removed *in vacuo* and the crude reaction residue purified by chromatography with a gradient of hexanes/DCM. The chromatographed material was redisolved into DCM and passed through a 0.2 µm syringe filter before removing the solvent *in vacuo* and recrystallizing from ethanol/THF mixtures.

2. Synthesis of Intermediates

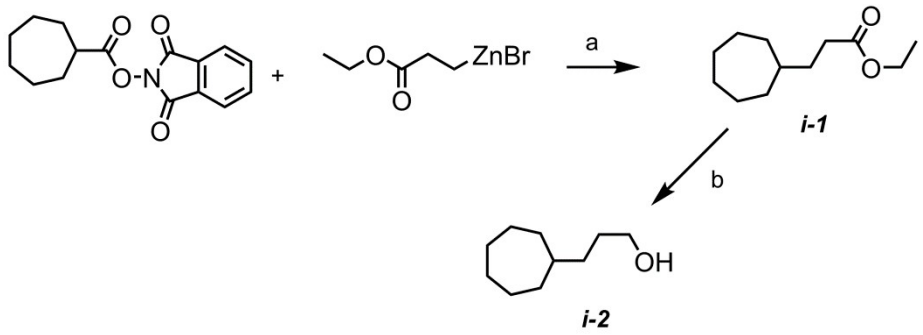

a... $NiCl_2$.glyme, dtbbpy, DMF/THF, Ar, 48 h
b... $LiAlH_4$, THF, Ar, 0.5 h

Scheme SI-1

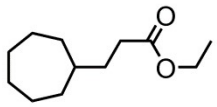

i-1: Ethyl 3-cycloheptylpropanoate

Nickel chloride ethyleneglycoldimethylether complex ($NiCl_2$.glyme, 0.1 mmol, 21.9 mg), 4,4′-ditertbutyl-2,2′-bipyridyl (dtbbpy, 53.6 mg, 0.2 mmol) and cycloheptyl NHPI-ester (1 mmol, 287 mg) were dissolved into freshly distilled DMF (6 ml) under an atmosphere of dry argon by stirring for 5 minutes, giving a turquoise solution. To this solution was added (3-ethoxy-3-oxypropyl)zinc bromide (3 mmol, 0.5 M in THF, 6 ml) in one portion prompting a colour change to red and then black. The solution was stirred and periodically monitored by TLC (staining with $KMnO_4$). The reaction was deemed complete upon complete consumption of the NHPI-ester ($Rf_{DCM} \approx 0.5$) and the formation of a new product ($Rf_{DCM} \approx 0.65$). The solvent was removed *in vacuo* and the target compound obtained as a colourless oil (with a sweet, fruity aroma) by flash chromatography with pentane/DCM as the eluent.

Spectral data was consistent with literature values. [8]

Yield: 130 mg (66 %)

Rf (DCM): 0.65

^{1}H NMR: 0.73 – 0.94 (1H, m, CyHept-H), 1.07 – 1.21 (2H, m, CyHept-H), 1.24 (3H, t, *J* = 7.3 Hz, COO-CH_2CH_3), 1.30 – 1.77 (12H, m, -CH_2- + CyHept-H), 2.27 (2H, t, *J* = 7.3 Hz, CyHept-CH_2CH_2-COO-), 4.10 (2H, Quartet, *J* = 7.3 Hz, COO-CH_2-CH_3)

^{13}C{^{1}H} NMR: 14.36, 26.44, 28.60, 32.60, 33.11, 34.31, 38.90, 60.27, 174.31

MS (ESI): 199.1696 (calcd. for $C_{12}H_{23}O_2$: 199.1693, M + H)
221.1519 (calcd. for $C_{12}H_{22}NaO_2$: 221.1512, M + Na)

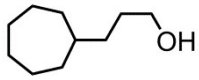

***i-2**:* 3-cycloheptylpropan-1-ol

i-1 (100 mg, 0.51 mmol) was dissolved into anhydrous THF (5 ml) under an atmosphere of dry argon. Solid $LiAlH_4$ (2 mmol, 74 mg) was added in one portion. The reaction was monitored by TLC; complete consumption of the starting material was noted after 30 minutes. The reaction was quenched with 1 ml of ethyl acetate (minor gas evolution) and the resulting suspension filtered through a pad of silica gel, which was subsequently washed with ethyl acetate (3 x 20 ml). The combined organics were concentrated *in vacuo* to afford the title compound as a viscous liquid with a foul odour.

Yield: 68 mg (93 %)

Rf (DCM): 0.37

^{1}H NMR: 1.10 – 1.30 (5H, m, CyHept<u>H</u> + -C<u>H$_2$</u>-), 1.33 – 1.70 (12H, m, CyHept<u>H</u> + -C<u>H$_2$</u>-), 3.62 (2H, t, *J* = 6.6 Hz, CH_2-C<u>H$_2$</u>-OH) *OH proton not observed*

^{13}C{^{1}H} NMR: 26.61, 28.56, 30.83, 34.21, 39.20, 63.58

MS (ESI): 157.1527 (calcd. for $C_{10}H_{20}O$: 157.1587, M + H)

3. Characterisation of Liquid-Crystalline Chemicals

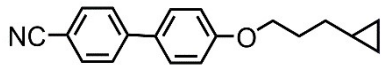

1: 4'-(3-cyclopropylpropoxy)-[1,1'-biphenyl]-4-carbonitrile

4-(Pent-4-enyloxy)-4′-cyanobiphenyl (506 mg, 2 mmol) was added to an oven dried flask and dissolved into the minimum quantity of anhydrous diethyl ether (~ 10 ml) at ambient temperature and under an atmosphere of dry argon. Diethyl zinc (6 mmol) was added in one portion and the solution stirred for 5 minutes. Diiodomethane (1.6 g, 483 µl, 6 mmol) was dissolved into anhydrous diethyl ether (total volume 20 ml, concentration ~ 0.3 M); this solution was then added to the reaction *via* a syringe pump at a rate of 0.1 ml min^{-1}. The solution became turbid, and was periodically monitored by ^{1}H NMR to determine the ratio of alkene to cyclopropane (the two materials could not be separated by TLC). After 18 h no alkene was present as judged from ^{1}H NMR and so the reaction was quenched with saturated aqueous ammonium chloride (5 ml). The aqueous layer was subsequently separated and discarded, the organic layer dried over magnesium sulphate and concentrated *in vacuo*. TLC analysis revealed two major components (Rf_{DCM} = 0.59 and Rf_{DCM} = 0.05) with numerous minor components. The crude reaction mixture was separated by flash chromatography with 5:3 hexanes/DCM as the eluent, recrystallization of the chromatographed material from methanol afforded the title compound as a white powder.

Yield: 290 mg (54 %)

Rf (TLC): 0.59 (DCM)

^{1}H NMR: 0.06 (2H, m, CyProp-H), 0.46 (2H, m, CyProp-H), 0.67 – 0.79 (1H, m, CH_2-CH-$(CH_2)_2$), 1.36 – 1.42 (2H, m, ArO-$(CH_2)_2$-CH_2-CyProp), 1.87 – 1.97 (2H, m, ArO-CH_2CH_2-CH_2-CyProp), 4.05 (2H, t, *J* = 6.4 Hz, ArO-CH_2-CH_2), 6.99 (2H, ddd, *J* = 2.2 Hz, *J* = 3.0 Hz, *J* = 8.8 Hz, ArH), 7.52 (2H, ddd, *J* = 2.2 Hz, *J* = 3.0 Hz, *J* = 8.8 Hz, ArH), 7.64 (2H, ddd, *J* = 1.8 Hz, *J* = 2.5 Hz, *J* = 8.2 Hz, ArH), 7.70 (2H, ddd, *J* = 1.8 Hz, *J* = 2.5 Hz, *J* = 8.2 Hz, ArH)

$^{13}C\{^{1}H\}$ NMR: 159.92, 145.43, 132.71, 131.38, 128.46, 127.21, 119.28, 115.21, 110.15, 67.93, 31.14, 29.39, 10.64, 4.62.

MS (ESI+): 278.1548 (calcd. for $C_{19}H_{20}NO$: 278.1539, M + H)
300.1368 (calcd. for $C_{19}H_{19}NNaO$: 300.1359, M + Na)

HPLC: 99.4%

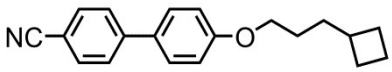

2: 4'-(3-cyclobutylpropoxy)-[1,1'-biphenyl]-4-carbonitrile

Under a flow of dry nitrogen gas, an oven dried Ace pressure tube equipped with a magnetic stirrer bar and front seal PTFE O-ring was charged with $Ir[dF(CF_3)ppy]_2(dtbbpy)PF_6$ (22.4 mg, 0.02 mmol), $NiCl_2$.glyme (21.9 mg, 0.1 mmol), 4-4′-ditertbutyl-2,2′-bipyridine (26.8 mg, 0.1 mmol), cyclobutanecarboxylic acid (150 mg, 1.5 mmol), caesium carbonate (650 mg, 2 mmol), ethyl acetate (3 ml) and acetonitrile (10 ml). The suspension was degassed by agitating in an ultrasonic bath whilst sparging with argon for 30 minutes. Degassed water (0.4 ml) was added, followed by 4-(3-bromopropyloxy)-4′-cyanobiphenyl (316 mg, 1 mmol). The tube was sealed under a positive pressure of argon, and the reaction mixture was vigorously stirred and irradiated with two LED banks (with peak output at 405 nm) for a period of 96 h. The reaction solution was filtered through a pad of celite and concentrated *in vacuo* to a yellow paste. The crude material was isolated by flash chromatography with 3:2 hexane/DCM as the eluent followed by recrystalisation from methanol, to afford the title compound as a white microcrystalline solid.

Yield: 122 mg (42 %)

Rf (TLC): 0.60 (DCM)

^{1}H NMR: 1.48 – 1.59 (2H, m, -CH_2-CH(-CH_2-)$_2$-C$\underline{H}_2$), 1.59 – 1.67 (2H, m, -CH_2-CH(-C$\underline{H}$H-)$_2$-CH_2), 1.67 – 1.80 (2H, m, -CH_2-CH(-CH$\underline{H}$-)$_2$-CH_2), 1.80 – 1.94 (2H, m, ArO-CH_2-CH_2-C$\underline{H}_2$-CyBu), 2.00 – 2.07 (2H, m, ArO-CH_2-C$\underline{H}_2$-CH_2-CyBu), 2.32 (1H, m, ArO-CH_2-CH_2-CH_2-C$\underline{H}$-$(CH_2)_2$-CH_2), 6.98 (2H, d, *J* = 7.9 Hz, Ar$\underline{H}$), 7.53 (2H , d, *J* = 7.9 Hz, Ar$\underline{H}$), 7.64 (2H, d, *J* = 8.1 Hz, Ar$\underline{H}$), 7.69 (2H, d, *J* = 8.1 Hz, Ar$\underline{H}$)

^{13}C{^{1}H} NMR: 18.55, 27.09, 28.46 ,33.35, 35.94, 68.28, 110.16, 115.20, 119.29, 127.22, 128.47, 131.39, 132.71, 145.44, 159.92

MS (ESI+): 292.1694 (calcd. for $C_{20}H_{22}NO$: 292.1696, M + H)
314.1525 (calcd. for $C_{20}H_{21}NNaO$: 314.1515, M + Na)

HPLC: >99.9%

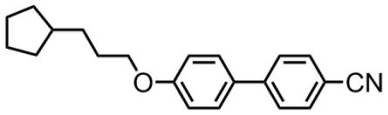

3: 4'-(3-cyclopentylpropoxy)-[1,1'-biphenyl]-4-carbonitrile

Quantities used: 4-hydroxy-4′-cyanobiphenyl (390 mg, 2 mmol), PPh_3 (629 mg, 2.4 mmol), 3-cyclopentylpropan-1-ol (256 mg, 2 mmol), DIAD (485 mg, 472 µl, 2.4 mmol), THF (20 ml). The general Mitsunobu procedure was followed, affording the title compound as long translucent needles.

Yield: 520 mg (75 %)

Rf (TLC): 0.54 (DCM)

^{1}H NMR: 1.04 – 1.19 (2H, m, CyPent-H), 1.42 – 1.69 (6H, m, Cypent-H + ArO-CH_2-CH_2-CH_2), 1.72 – 1.90 (5H, m, ArO-CH_2-CH_2-CH_2 + CyPent-H), 4.01 (2H, t, *J* = 7.0 Hz, ArO-CH_2-CH_2-), 6.98 (2H, ddd, *J* = 2.0 Hz, *J* = 2.8 Hz, *J* = 8.8 Hz, ArH), 7.52 (2H, ddd, *J* = 2.0 Hz, *J* = 2.8 Hz, *J* = 8.9 Hz, ArH), 7.63 (2H, ddd, *J* = 2.0 Hz, *J* = 2.5 Hz, *J* = 8.2 Hz, ArH), 7.68 (2H, ddd, *J* = 2.0 Hz, *J* = 2.5 Hz, *J* = 8.2 Hz, ArH)

^{13}C NMR: 25.30, 28.57, 32.51, 32.80, 40.00, 68.49, 110.09, 115.16, 119.24, 127.15, 128.41, 131.30, 132.65, 145.37, 159.90,

MS (ESI+): 306.1866 (calcd. for $C_{21}H_{24}NO$: 306.1852, M + H)
328.1683 (calcd. for $C_{21}H_{23}NNaO$: 328.1672, M + Na)

HPLC: > 99.9%

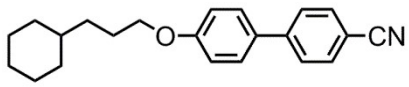

4: 4'-(3-cyclohexylpropoxy)-[1,1'-biphenyl]-4-carbonitrile

Quantities used: 4-hydroxy-4′-cyanobiphenyl (390 mg, 2 mmol), PPh_3 (629 mg, 2.4 mmol), 3-cyclohexylpropan-1-ol (284 mg, 2 mmol), DIAD (485 mg, 472 µl, 2.4 mmol), THF (20 ml). The general Mitsunobu protocol was followed, affording the title compound as a colourless crystalline solid.

Yield: 590 mg (92 %)

Rf (TLC): 0.54 (DCM)

^{1}H NMR: 7.69 (d, J = 8.2 Hz, 2H), 7.64 (d, J = 8.2 Hz, 2H), 7.52 (d, J = 8.7 Hz, 2H), 6.99 (d, J = 8.6 Hz, 2H), 3.99 (t, J = 6.6 Hz, 2H), 1.91 – 1.78 (m, 2H), 1.68 (m, 5H), 1.42 – 1.31 (m, 2H), 1.31 – 1.09 (m, 4H), 1.02 – 0.83 (m, 2H).

^{13}C{^{1}H} NMR: 159.94, 145.44, 132.70, 131.37, 128.45, 127.21, 119.28, 115.22, 110.14, 68.68, 37.59, 33.80, 33.47, 26.79, 26.73, 26.50.

MS (ESI+): 342.1844 (calcd for $C_{22}H_{25}NNaO$:342.1828, M + Na)

HPLC: >99.9%

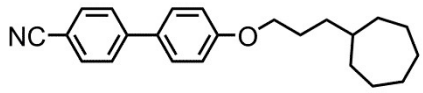

5: 4'-(3-cycloheptylpropoxy)-[1,1'-biphenyl]-4-carbonitrile

Quantities used: 4-hydroxy-4′-cyanobiphenyl (97.5 mg, 0.5 mmol), PPh_3 (262 mg, 1 mmol), 3-cyclopentylpropan-1-ol (***i-2***, 40 mg, 0.26 mmol), DIAD (202 mg, 196 µl, 1 mmol), THF (2 ml). The general Mitsunobu procedure was followed, affording the title compound as colourless plates following recrystalisation from neat ethanol.

Yield: 55 mg (64%)

Rf (TLC): 0.59 (DCM)

^{1}H NMR: 1.13 – 1.27 (2H, m, CyHept-H), 1.33 -1.77 (13H, m, CyHept-H + -CH_2-), 1.77 – 1.87 (2H, m, CyHept-CH_2-CH_2-CH_2OAr), 3.98 (2H, t, *J* = 7.0 Hz, ArO-CH_2-CH_2-CH_2-), 6.99 (2H, ddd, *J* = 2.1 Hz, *J* = 2.8 Hz, *J* = 8.8 Hz, ArH), 7.53 (2H, ddd, *J* = 2.1 Hz, *J* = 2.8 Hz, *J* = 8.9 Hz, ArH), 7.64 (2H, ddd, *J* = 2.0 Hz, *J* = 2.5 Hz, *J* = 8.4 Hz, ArH), 7.69 (2H, ddd, *J* = 2.0 Hz, *J* = 2.5 Hz, *J* = 8.4 Hz, ArH)

^{13}C NMR: 26.61, 27.25, 28.63, 34.45, 34.67, 39.16, 68.66, 110.12, 115.19, 119.27, 127.19, 128.44, 131.34, 132.69, 145.41, 159.91

MS (ESI+): 334.2175 (calcd. for $C_{23}H_{28}NO$: 334.2165, M + H)
356.2001 (calcd. for $C_{23}H_{27}NNaO$: 356.1985, M + Na)

HPLC: 98.9%

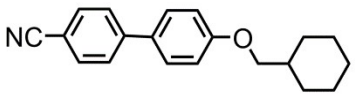

6: 4'-(cyclohexylmethoxy)-[1,1'-biphenyl]-4-carbonitrile

Quantities used: 4-hydroxy-4′-cyanobiphenyl (975 mg, 5 mmol), PPh_3 (1.6 g, 6 mmol), cyclohexylmethanol (684 mg, 6 mmol), DIAD (1.2 g, 1.2 ml, 6 mmol), THF (25 ml). The general experimental procedure was followed, affording the title compound as large colourless crystals following recrystalisation from ethanol.

Yield: 1.3 g (89 %)

Rf (TLC): 0.51 (DCM)

^{1}H NMR 1.07 (2H, qd, *J* = 3.2 Hz, *J* = 12.3 Hz, CyH), 1.14 – 1.38 (3H, m, CyH), 1.65 – 1.94 (6H, m, CyH), 3.80 (2H, d, *J* = 6.4 Hz, ArOCH$_2$-Cy), 6.99 (2H, ddd, *J* = 2.2 Hz, *J* = 3.0 Hz, *J* = 9.2 Hz, ArH), 7.52 (2H, ddd, *J* = 2.2 Hz, *J* = 3.0 Hz, *J* = 9.2 Hz, ArH), 7.63 (2H, ddd, *J* = 1.8 Hz, *J* = 2.2 Hz, *J* = 8.2 Hz, ArH), 7.69 (2H, ddd, *J* = 1.8 Hz, *J* = 2.2 Hz, *J* = 8.2 Hz, ArH)

^{13}C{^{1}H} NMR: 160.01, 145.26, 132.55, 131.11, 128.30, 127.03, 119.15, 115.09, 109.96, 73.62, 37.69, 29.90, 26.53, 25.82.

MS (ESI+): 292.1707 (calcd for $C_{20}H_{22}NO$: 292.1696, M + H)
314.1529 (calcd. for $C_{20}H_{21}NNaO$: 314.1515, M + Na)

HPLC: >99.9%

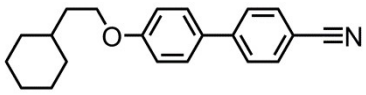

7: 4'-(2-cyclohexylethoxy)-[1,1'-biphenyl]-4-carbonitrile

Quantities used: 4-hydroxy-4′-cyanobiphenyl (975 mg, 5 mmol), PPh_3 (1.6 g, 6 mmol), 2-cyclohexylethanol (768 mg, 6 mmol), DIAD (1.2 g, 1.2 ml, 6 mmol), THF (25 ml). The general experimental procedure was followed, affording the title compound as a colourless needles following recrystalisation from ethanol.

Yield: 1.4 g (92 %)

Rf (TLC): 0.48 (DCM)

^{1}H NMR 0.99 (2H, qd, *J* = 2.6 Hz, *J* = 12.2 Hz, CyH), 1.08– 1.39 (3H, m, CyH), 1.53 (1H, tquintet, *J* = 3.4 Hz, *J* = 7.0 Hz, CyH-CH_2), 1.62 – 1.83 (7H, m, CyH + ArO-CH_2-CH_2-Cy), 4.04 (2H, d, *J* = 7.0 Hz, ArOCH_2-CH_2-Cy), 7.00 (2H, ddd, *J* = 2.1 Hz, *J* = 3.0 Hz, *J* = 9.2 Hz, ArH), 7.52 (2H, ddd, *J* = 2.1 Hz, *J* = 3.0 Hz, *J* = 9.2 Hz, ArH), 7.62 (2H, ddd, *J* = 1.8 Hz, *J* = 2.5 Hz, *J* = 8.4 Hz, ArH), 7.67 (2H, ddd, *J* = 1.8 Hz, *J* = 2.5 Hz, *J* = 8.4Hz, ArH)

^{13}C{^{1}H} NMR: 159.81, 145.23, 132.54, 131.15, 128.30, 127.03, 119.13, 115.08, 109.97, 66.12, 36.59, 34.54, 33.31, 26.54, 26.26.

MS (ESI+): 328.1685 (calcd for $C_{21}H_{23}NNaO$:328.1672, M + Na)

HPLC: 99.7%

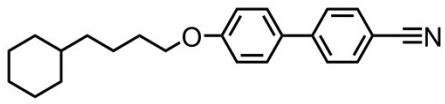

8: 4'-((4-cyclohexylbutyl)oxy)-[1,1'-biphenyl]-4-carbonitrile

Quantities used: 4-hydroxy-4′-cyanobiphenyl (390 mg, 2 mmol), PPh_3 (629 mg, 2.4 mmol), 4-cyclohexylbutan-1-ol (312 mg, 2 mmol), DIAD (485 mg, 472 µl, 2.4 mmol), THF (20 ml). The general Mitsunobu protocol was followed, affording the title compound as a colourless crystalline solid.

Yield: 510 mg (77%)

Rf (TLC): 0.51 (DCM)

^{1}H NMR: 0.80 – 0.96 (2H, m, CyH), 1.11 – 1.30 (6H, m, CyH), 1.42 – 1.54 (2H, m, CyH), 1.60 – 1.86 (7H, m, CyH + ArO-CH_2-CH_2), 4.00 (2H, d, *J* = 6.6 Hz, ArOCH_2-CH_2), 6.99 (2H, ddd, *J* = 1.8 Hz, *J* = 2.5 Hz, *J* = 8.8 Hz, ArH), 7.52 (2H, ddd, *J* = 1.8 Hz, *J* = 2.5 Hz, *J* = 8.8 Hz, ArH), 7.62 (2H, ddd, *J* = 2.1 Hz, *J* = 2.5 Hz, *J* = 8.8 Hz, ArH), 7.67 (2H, ddd, *J* = 2.1 Hz, *J* = 2.5 Hz, *J* = 8.8Hz, ArH)

^{13}C{^{1}H} NMR: 159.90, 145.35, 132.63, 131.27, 128.39, 127.13, 119.22, 115.16, 110.07, 68.26, 37.69, 37.29, 33.47, 29.60, 26.80, 26.51, 23.40.

MS (ESI+): 334.2176 (calcd. for $C_{23}H_{28}NO$: 334.2165, M + H)
356.1999 (calcd. for $C_{23}H_{27}NNaO$: 356.1985, M + Na)

HPLC: 99.6%

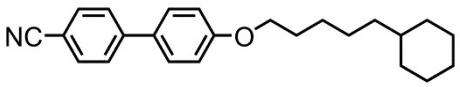

9: 4'-((5-cyclohexylpentyl)oxy)-[1,1'-biphenyl]-4-carbonitrile

Quantities used: 4-hydroxy-4′-cyanobiphenyl (390 mg, 2 mmol), PPh_3 (629 mg, 2.4 mmol), 5-cyclohexylpentan-1-ol (340 mg, 2 mmol), DIAD (485 mg, 472 µl, 2.4 mmol), THF (20 ml). The general Mitsunobu protocol was followed, affording the title compound as a colourless crystalline solid.

Yield: 570 mg (82 %)

Rf (TLC): 0.52 (DCM)

^{1}H NMR: 0.75 – 0.97 (2H, m, Cy<u>H</u>), 1.05 – 1.30 (6H, m, Cy<u>H</u> + -CH_2-C<u>H</u>$_3$), 1.30 – 1.53 (4H, m, Cy<u>H</u> + -CH_2-C<u>H</u>$_2$-CH_3), 1.59 – 1.74 (5H, m, Cy<u>H</u> + ArO-CH_2-CH_2-C<u>H</u>$_2$-CH_2-), 1.76 – 1.91 (2H, m, ArO-CH_2-C<u>H</u>$_2$-CH_2), 4.00 (2H, d, *J* = 6.6 Hz, ArO-C<u>H</u>$_2$-CH_2), 6.99 (2H, ddd, *J* = 2.1Hz, *J* = 2.5 Hz, *J* = 8.8 Hz, Ar<u>H</u>), 7.52 (2H, ddd, *J* = 2.1 Hz, *J* = 2.5 Hz, *J* = 8.8 Hz, Ar<u>H</u>), 7.62 (2H, ddd, *J* = 2.1 Hz, *J* = 2.5 Hz, *J* = 9.1 Hz, Ar<u>H</u>), 7.67 (2H, ddd, *J* = 2.1 Hz, *J* = 2.5 Hz, *J* = 9.2 Hz, Ar<u>H</u>)

^{13}C{^{1}H} NMR: 159.88, 145.32, 132.61, 131.24, 128.37, 127.10, 119.19, 115.14, 110.05, 68.23, 37.68, 37.50, 33.51, 29.32, 26.81, 26.70, 26.51, 26.42.

MS (ESI+): 348.2326 (calcd. for $C_{24}H_{30}NO$: 348.2322, M + H)
370.2156 (calcd. for $C_{24}H_{29}NNaO$: 370.2141, M + Na)

HPLC: 99.3%

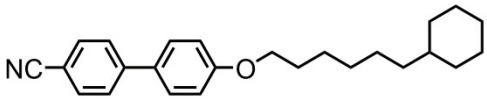

10: 4'-((6-cyclohexylhexyl)oxy)-[1,1'-biphenyl]-4-carbonitrile

Quantities used: 4-hydroxy-4′-cyanobiphenyl (195 mg, 1 mmol), PPh_3 (524 mg, 2 mmol), 6-cyclohexylhexan-1-ol (368 mg, 2 mmol), DIAD (404 mg, 393 µl, 2.4 mmol), THF (4 ml). The general Mitsunobu protocol was followed, affording the title compound as a colourless crystalline solid following recrystalisation from nitromethane.

Yield: 281 mg (75%)

Rf (TLC): 0.61 (DCM)

^{1}H NMR: 0.75 – 0.93 (2H, m, Cy<u>H</u>), 1.05 – 1.26 (6H, m, Cy<u>H</u> + -CH_2-C<u>H</u>$_2$), 1.27 – 1.38 (4H, m, Cy<u>H</u> + -CH_2-C<u>H</u>$_2$-CH_2), 1.39 – 1.50 (2H, m, -CH_2-C<u>H</u>$_2$-CH_2), 1.60 – 1.72 (5H, m, Cy<u>H</u> + ArO-CH_2-CH_2-C<u>H</u>$_2$-CH_2-), 1.75 – 1.88 (2H, m, ArO-CH_2-C<u>H</u>$_2$-CH_2), 3.99 (2H, d, *J* = 6.6 Hz, ArO-C<u>H</u>$_2$-CH_2), 6.98 (2H, ddd, *J* = 1.8 Hz, *J* = 2.4 Hz, *J* = 8.8 Hz, Ar<u>H</u>), 7.52 (2H, ddd, *J* = 1.8 Hz, *J* = 2.4 Hz, *J* = 8.8 Hz, Ar<u>H</u>), 7.63 (2H, ddd, *J* = 2.1 Hz, *J* = 2.4 Hz, *J* = 9.1 Hz, Ar<u>H</u>), 7.68 (2H, ddd, *J* = 2.1 Hz, *J* = 2.4 Hz, *J* = 9.2 Hz, Ar<u>H</u>)

^{13}C{^{1}H} NMR: 26.19, 26.59, 26.89, 26.91, 29.35, 29.84, 33.59, 37.60, 37.79, 68.33, 110.15, 115.22, 119.27, 127.21, 128.45, 131.37, 132.70, 145.44, 159.94

MS (APCI+): 362.248399 (calcd. for $C_{25}H_{32}NO$: 362.247841, M + H)

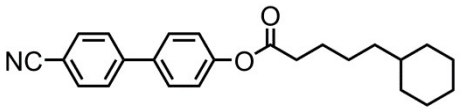

11: 4'-cyano-[1,1'-biphenyl]-4-yl 5-cyclohexylpentanoate

5-Cyclohexylpentanoic acid (1 g, 5.4 mmol) was added dropwise to a suspension of 4-hydroxy-4′-cyanobiphenyl (970 mg, 5 mmol), EDAC.HCl (1.1 g, 6 mmol) and DMAP (50 mg) in dichloromethane. The suspension was vigorously stirred and became a homogenous solution within a few minutes. Stirring was continued for 1 h, the solvent was removed *in vacuo* and the crude residue was purified by flash chromatography with a gradient of hexanes/DCM. The chromatographed material was redisolved into DCM and passed through a 0.2 µm syringe filter before removing the solvent *in vacuo* and recrystallizing from ethanol/THF mixtures.

Yield: 1.7 g (94 %)

Rf (TLC): 0.46 (DCM)

^{1}H NMR: 0.78 – 0.97 (2H, m, Cy$\underline{H}$), 1.07 – 1.37 (6H, m, -CH_2-$C\underline{H}_3$ + Cy$\underline{H}$), 1.38 – 1.50 (2H, m, -CH_2-$C\underline{H}_2$-CH_2-CH_3), 1.59 – 1.83 (7H, m, ArCOO-$CH_2C\underline{H}_2$-CH_2 + Cy$\underline{H}$), 2.59 (2H, t, *J* = 7.5 Hz, ArCOO-$C\underline{H}_2$-CH_2-), 7.20 (2H, d, *J* = 8.6 Hz, Ar$\underline{H}$), 7.59 (2H, d, *J* = 8.6 Hz, Ar$\underline{H}$, 7.65 (2H, d, *J* = 8.4 Hz, Ar$\underline{H}$), 7.71 (2H, d, *J* = 8.4 Hz, Ar$\underline{H}$)

^{13}C{^{1}H} NMR: 172.33, 151.30, 144.85, 136.79, 132.72, 128.39, 127.74, 122.43, 118.95, 111.06, 37.54, 37.15, 34.51, 33.46, 26.78, 26.48, 26.44, 25.29.

MS (ESI+): 384.1948 (calcd. for $C_{25}H_{31}NNaO$: 384.1934, M + Na)

HPLC: 99.8%

4. Supplemental Data

4.1. Supplemental SAXS data

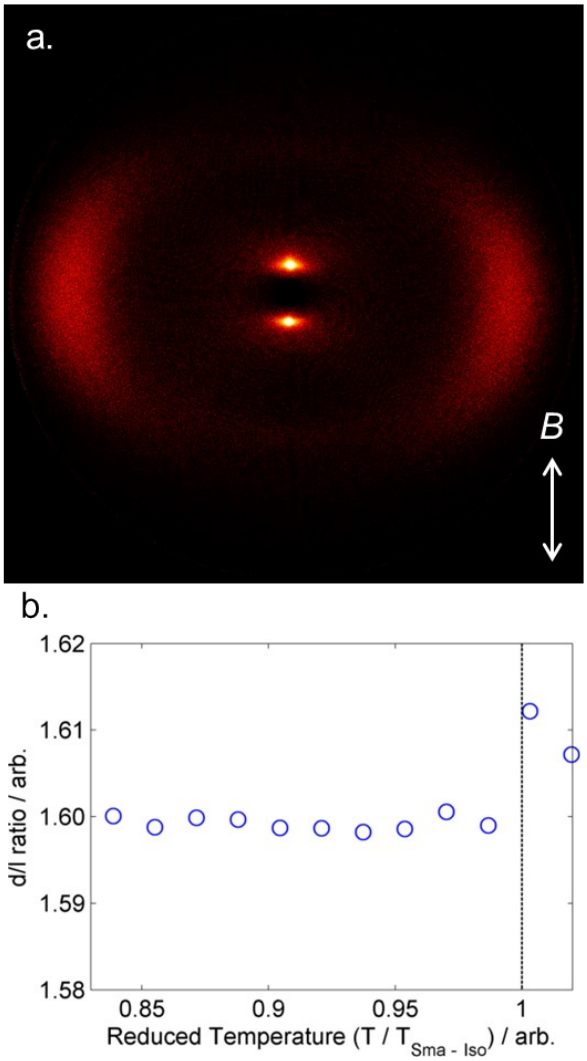

Figure SI-1: (a) two dimensional SAXS pattern obtained for a magnetically aligned sample of compound **11** at a temperature of 65 °C, (b) plot of the d/l ratio of compound **11** as a function of reduced temperature ($T / T_{SmA\text{-}N}$) using the molecular length of 21.4 Å obtained from the B3LYP/6-31G(d) minimised geometry of **11**.

4.2. Supplemental Microscopy Data

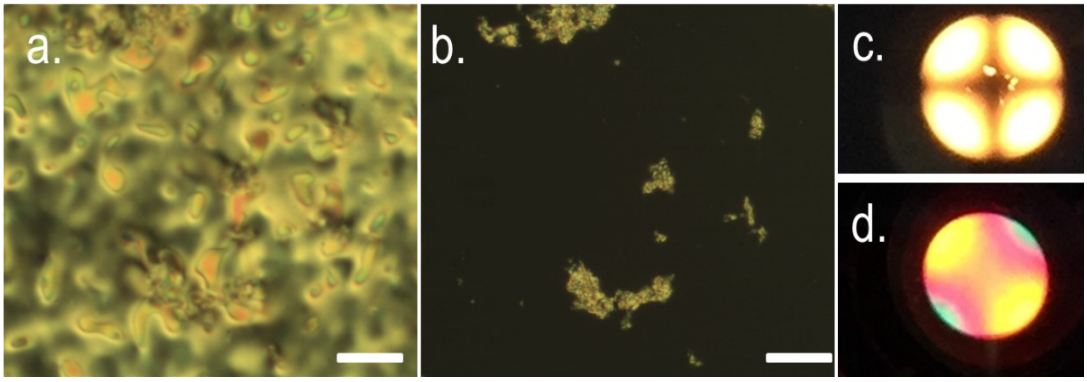

Figure SI-2: Photomicrographs (x100, scale bar 100 µm) of the nematic phase (a, 53 °C) and the smectic A phase (47 °C) of compound **8**. (c) Conoscopic figure obtained for the smectic A phase demonstrating the phase to be uniaxial, insertion of a ¼ wave plate (d) demonstrates the phase to be optically positive.

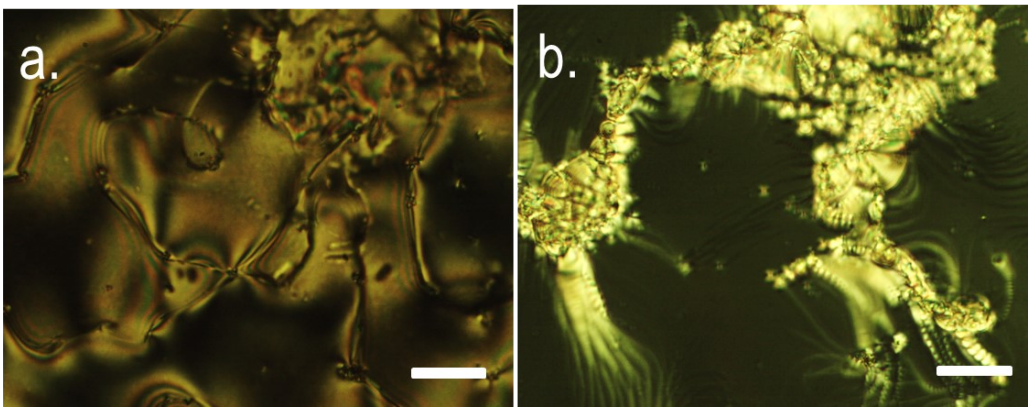

Figure SI-3: Photomicrographs (x100, scale bar 100 µm) of the nematic phase (a, 84.3 °C) and the smectic A phase (79.5 °C) of compound **9**.

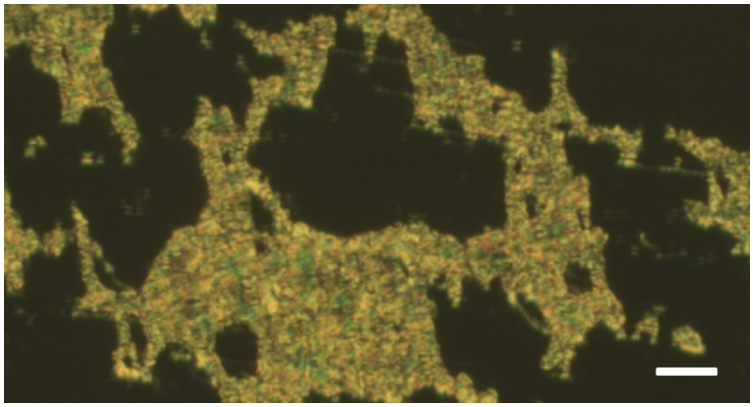

Figure SI-4: Photomicrograph (x100, scale bar 100 µm) of the smectic A phase of **10** at 66 °C

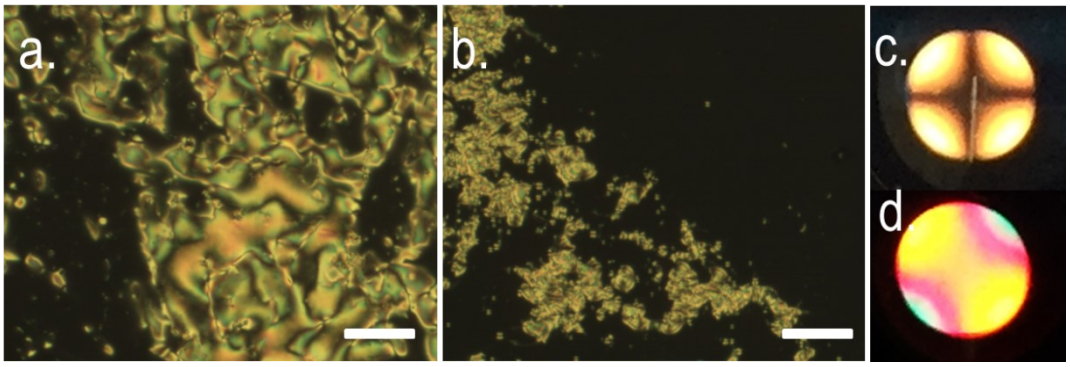

Figure SI-5: Photomicrographs (x100, scale bar 100 µm) of the nematic phase (a, 70 °C) and the smectic A phase (62 °C) of compound **5**. (c) Conoscopic figure obtained in the smectic A phase demonstrating the phase to be uniaxial, insertion of a ¼ wave plate (d) demonstrates the phase to be optically positive.

5. Molecular dynamics simulations: methods and supplemental data

Initial geometries for simulations were prepared by further optimising the all-trans conformers of 8OCB and **9** at the B3LYP/6-31++G(d,p) level [9, 10] using Gaussian 16 Rev A.03. [11] Electrostatic potentials were then calculated at the HF/6-31++G(d,p) level using Gaussian 16, before using AmberTools 19[12] to generate a set of RESP[13] atomic charges and a set of GAFF version 1.81 forcefield parameters.[14] The forcefield parameters were then converted using ACPYPE[15] and some forcefield parameters, namely the C-C-C-C torsional parameters and the non-bonded parameters for aromatic carbon atoms, were modified to those reported to give improved results for liquid crystal molecules.[16] Fully atomistic molecular dynamics (MD) simulations were then performed with GROMACS 2019.3.[17-23]

All MD simulations were run with periodic boundary conditions using 2-fs steps, and all bonds were constrained at their equilibrium lengths using the LINCS algorithm.[24] A van der Waals cutoff of 1.2 nm was used, and the Particle Mesh Ewald method[25] was used for long-range electrostatic interactions with a cutoff of 1.2 nm. Coordinates were written to trajectory files every 50 ps for the main simulations. For the system preparation and equilibration steps, a velocity rescaling thermostat[26] and Berendsen barostat[27] were used, as appropriate; for the full simulations, a Nose-Hoover thermostat[28, 29] with a 1-ps time constant and a Parrinello-Rahman barostat[30, 31] with a 4-ps time constant were used. Dispersion correction was used for energy and pressure, and simulation trajectories were visualised in VMD 1.9.4.[32]

Initial simulation boxes were prepared by arranging molecules onto a regular 3D grid at a spacing corresponding to a gas-phase density (<20 kg m^{-3}), and doing a simulation run to allow the system to randomise, before it was compressed to a liquid-phase density (ca. 1,000 kg m^{-3}).

In order to estimate a clearing point in these MD simulations of 8OCB and **9**, a series of small simulations of 6 × 6 × 6 = 216 molecules were performed. Each system was allowed to randomise for 40 ps at low density at 298 K with no pressure coupling (final P_2 = 0.1), and then it was compressed rapidly at a nominal pressure of 50,000 bar until a liquid-like density was reached. The condensed, randomised phase was allowed to stabilise at 1 bar, before equilibrating at 353 K (8OCB) or 358 K (**9**). A 500-ns simulation was then run, during which each system formed a fairly stable smectic A phase. Subsequently, 100-ns simulations were run from the final coordinates at a range of temperatures at ca. 10 K intervals both higher and lower than those at which the 500-ns run had been performed, and with isotropic pressure coupling at 1 bar. The orientational order parameters (P_2) determined as a function of temperature (T) were fitted to a Haller type equation, $P_2 = [1 - (T/T_c)]^{\beta}$, where T_c gives an estimate of the clearing point of the system in the simulation and β is an empirical parameter. The data and fits from these small simulations are shown in Figure SI-6, and gave estimated T_c values of ca. 395 and 400 K for 8OCB and **9**, respectively, in these simulated systems.

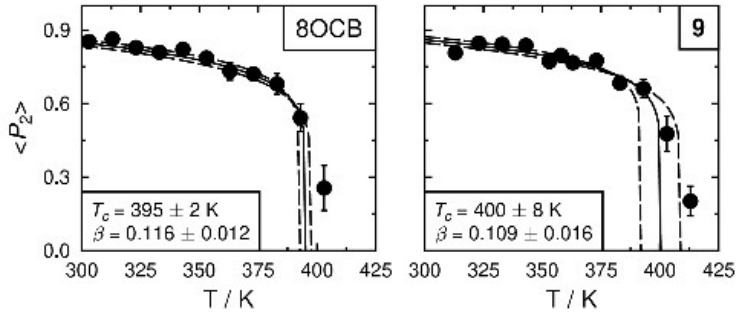

Figure SI-6. Orientational order parameters, P_2, averaged over 80–100 ns of the small MD simulations of 8OCB (left) and **9** (right) shown as markers, overlaid with fits (solid lines) and 95% confidence limits shown by dashed lines. Error bars represent the standard deviation over the sampled time range of the MD simulation.

The larger simulations presented in the main text were performed at temperatures of 369 and 374 K for 8OCB and Cyc-5OCB, respectively, both corresponding to $T/T_c \approx 0.934$, which was chosen to be in the experimental smectic A range for 8OCB. Each of the larger runs was prepared as a low-density 3D grid of 12 × 12 × 10 = 1440 molecules in an approximately cubic simulation box. The initial, ordered system was simulated for 70 ps at a nominal pressure of 10 bar to allow the system to randomise (final $P_2 = 0.04$), and it was then compressed at a nominal pressure of 50,000 bar until a liquid-like density was reached. The system was then allowed to stabilise at 1 bar and the desired simulation temperature before running the final simulations. These simulations used anisotropic pressure coupling to allow the simulation box to change aspect ratio as the simulation progressed, such that the phase formed was not biased by a simulation box with a fixed aspect ratio.

Second-rank orientational order parameters, P_2, were calculated for each trajectory frame as −2× the middle eigenvalue of the ordering tensor, $Q_{\alpha\beta}$, defined by Equation 1, where N is the number of molecules, j is the molecule number in the simulation, α and β represent the Cartesian x, y and z axes, δ is the Kronecker delta, and a is the component of the principal molecular axis vector defined in the text. The director at each frame was defined as the eigenvector associated with the largest eigenvalue of the ordering tensor.

$$Q_{\alpha\beta} = \frac{1}{N}\sum_{j=1}^{N}\frac{3a_{j\alpha}a_{j\beta} - \delta_{\alpha\beta}}{2} \qquad (1)$$

The overall layer-normal vector was determined using a set of N local layer-normal vectors determined using a suitable reference atom in each molecule, as identified in the main text. The local layer-normal vector of each molecule was determined by combining the reference atom position with those of the equivalent reference atoms in surrounding molecules that were within a cutoff distance of 1 nm, fitting a plane through the set of reference atoms, and then the local layer-normal vector is a normal vector to that plane. The overall layer-normal vector was then determined for each trajectory frame as the eigenvector associated with the largest eigenvalue of an ordering tensor equivalent to Equation 1 but assembled from the set of local layer-normal vectors determined for that frame.

The translational order parameter, τ, was then determined using the distribution of a suitable reference atom within the molecules along the overall layer-normal vector using Equation 2,[33] where z is the position of a reference atom projected onto the overall layer-normal vector, d is the layer spacing, which is optimised to give the highest value of τ for each trajectory frame, L is the length of the box used in the analysis, and the angular brackets denote an ensemble average for that frame.

$$\tau = \sqrt{\left[\left\langle \cos\left(\frac{2\pi z}{d}\right)\right\rangle - \frac{d}{2\pi L}\sin\left(\frac{2\pi L}{d}\right)\right]^2 + \left\langle \sin\left(\frac{2\pi z}{d}\right)\right\rangle^2} \qquad (2)$$

For the large simulations presented in the main text, the angle, $\theta_{\mathbf{nk}}$, between the director, **n**, and the layer normal vector, **k**, was determined for each frame. Normalised orientational distribution functions for this angle, $f(\theta_{\mathbf{nk}})$, were calculated by dividing the populations of these angles by $\sin(\theta_{\mathbf{nk}})$, and are shown in Figure SI-7. The orientational distribution functions for 8OCB and **9** have their highest values at <2°, indicating that the director tends to align with the layer normal in both simulations, corresponding to smectic A phases, whereas smectic C phases would give a maximum significantly greater than 0°. The orientational distribution function is narrower for **9** than for 8OCB, consistent with a more ordered phase.

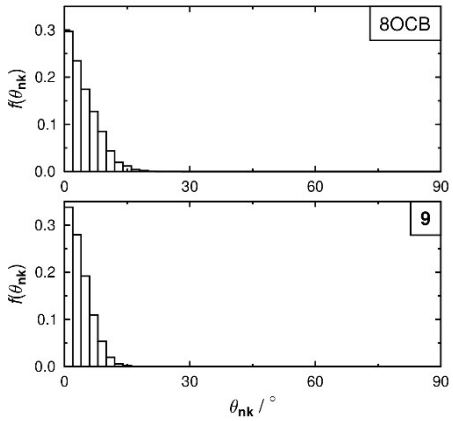

Figure SI-7. Orientational distribution functions, $f(\theta_{\mathbf{nk}})$, determined for 8OCB (top) and **9** (bottom) from the MD simulations, averaged over 60–200 ns and 200–1000 ns, respectively, using 2 ° binwidths.

The radial distribution function, $g(r)$ (Equation 3) reports on the relative probability of distances, r_{ij}, between a reference point on molecule i and the equivalent point on molecule j, ρ_N is the average number density of the system, and δ is the Dirac Delta function. Orientational correlation functions $G_1(r)$ and $G_2(r)$, Equations 4 and 5, respectively, report on the relative orientations between pairs of molecules,[32] where θ_{ij} is the angle between a reference vector on molecule i and the equivalent vector on another molecule, j. In this study, $g(r)$, $G_1(r)$, and $G_2(r)$ were determined using vectors defined between the carbon atoms at the 4 and 4′ positions of the biphenyl moieties, and distances, r_{ij}, were determined between the centre points of these two vectors.

$$g(r) = \frac{1}{4\pi r^2 r_N} \left\langle \delta(r - r_{ij}) \right\rangle_{ij} \quad (3)$$

$$G_1(r) = \frac{\left\langle \delta(r - r_{ij}) \cos\theta_{ij} \right\rangle_{ij}}{\left\langle \delta(r - r_{ij}) \right\rangle_{ij}} \quad (4)$$

$$G_2(r) = \frac{\left\langle \delta(r - r_{ij}) P_2(\cos\theta_{ij}) \right\rangle_{ij}}{\left\langle \delta(r - r_{ij}) \right\rangle_{ij}} \quad (5)$$

6. Supplementary XRD data

6.1. Structure Determination by Single Crystal XRD

Diffraction data were collected at 110 K on an Oxford Diffraction SuperNova diffractometer with Cu-K_α radiation (λ = 1.54184 Å) using an EOS CCD camera. The crystal was cooled with an Oxford Instruments Cryojet. Diffractometer control, data collection, initial unit cell determination, frame integration and unit-cell refinement was carried out with "Crysalis". [35] Face-indexed absorption corrections were applied using spherical harmonics, implemented in SCALE3 ABSPACK scaling algorithm.[36] OLEX2 [37] was used for overall structure solution, refinement and preparation of computer graphics and publication data. Within OLEX2, the algorithm used for structure solution was ShelXT [38] using intrinsic phasing. Refinement by full-matrix least-squares used the SHELXL[39] algorithm within OLEX2.[37] All non-hydrogen atoms were refined anisotropically. Hydrogen atoms were placed using a "riding model" and included in the refinement at calculated positions.

6.2. XRD Data for Compound 1

Single crystals of $C_{19}H_{19}NO$ (compound **1**) were obtained by diffusion of ethanol and water into a DCM solution of **1**.

Crystal structure determination of 1

Crystal Data for $C_{19}H_{19}NO$ (M =277.35 g/mol): triclinic, space group P-1 (no. 2), a = 5.4374(3) Å, b = 10.4374(4) Å, c = 13.6579(6) Å, α = 104.161(4)°, β = 92.138(4)°, γ = 95.945(4)°, V = 745.94(6) Å^3, Z = 2, T = 110.05(10) K, μ(CuKα) = 0.589 mm^{-1}, *Dcalc* = 1.235 g/cm^3, 13771 reflections measured (8.798° ≤ 2Θ ≤ 142.356°), 2867 unique (R_{int} = 0.0343, R_{sigma} = 0.0251) which were used in all calculations. The final R_1 was 0.0410 (I > 2σ(I)) and wR_2 was 0.1119 (all data).

6.3. XRD Data for Compound 2

Single crystals of $C_{20}H_{21}NO$ (compound **2**) were obtained by slow evaporation of an ethanol solution.

Crystal structure determination of 2

Crystal Data for $C_{20}H_{21}NO$ (*M* =291.38 g/mol): triclinic, space group P-1 (no. 2), *a* = 5.6557(4) Å, *b* = 10.2172(9) Å, *c* = 14.8788(10) Å, *α* = 70.217(7)°, *β* = 81.954(6)°, *γ* = 88.731(6)°, *V* = 800.78(11) Å^3, *Z* = 2, *T* = 110.05(10) K, μ(CuKα) = 0.572 mm^{-1}, *Dcalc* = 1.208 g/cm^3, 4627 reflections measured (9.202° ≤ 2Θ ≤ 134.158°), 2832 unique (R_{int} = 0.0217, R_{sigma} = 0.0343) which were used in all calculations. The final R_1 was 0.0456 (I > 2σ(I)) and wR_2 was 0.1288 (all data).

6.4. XRD Data for Compound 3

Single crystals of $C_{21}H_{23}NO$ (compound **3**) were obtained by diffusion of ethanol into a DCM solution of **3**.

Crystal structure determination of 3

Crystal Data for $C_{21}H_{23}NO$ (*M* =305.40 g/mol): monoclinic, space group $P2_1/n$ (no. 14), *a* = 12.1243(2) Å, *b* = 6.58920(10) Å, *c* = 21.5514(3) Å, *β* = 105.406(2)°, *V* = 1659.86(5) Å^3, *Z* = 4, *T* = 110.05(10) K, μ(CuKα) = 0.574 mm^{-1}, *Dcalc* = 1.222 g/cm^3, 11210 reflections measured (7.63° ≤ 2Θ ≤ 134.134°), 2962 unique (R_{int} = 0.0222, R_{sigma} = 0.0164) which were used in all calculations. The final R_1 was 0.0397 (I > 2σ(I)) and wR_2 was 0.1093 (all data).

6.5. XRD Data for Compound 4

Single crystals of $C_{22}H_{25}NO$ (compound **4**) were obtained by slow evaporation of an ethanol solution of **4.**

Crystal structure determination of 4

Crystal Data for $C_{22}H_{25}NO$ (*M* =319.43 g/mol): triclinic, space group P-1 (no. 2), *a* = 7.0753(4) Å, *b* = 9.7137(5) Å, *c* = 13.3506(8) Å, *α* = 78.906(5)°, *β* = 83.156(5)°, *γ* = 82.858(5)°, *V* = 889.13(9) Å^3, *Z* = 2, *T* = 110.05(10) K, μ(CuKα) = 0.556 mm^{-1}, *Dcalc* = 1.193 g/cm^3, 5477 reflections measured (6.78° ≤ 2Θ ≤ 134.158°), 3180 unique (R_{int} = 0.0189, R_{sigma} = 0.0285) which were used in all calculations. The final R_1 was 0.0406 (I > 2σ(I)) and wR_2 was 0.1138 (all data).

6.6. XRD Data for Compound 5

Single crystals of $C_{23}H_{27}NO$ (compound **5**) were obtained by diffusion of ethanol into a DCM solution of **5**.

Crystal structure determination of compound 5

Crystal Data for $C_{23}H_{27}NO$ (*M* =333.45 g/mol): triclinic, space group P-1 (no. 2), *a* = 7.4340(6) Å, *b* = 9.3359(6) Å, *c* = 13.7657(9) Å, *α* = 80.118(6)°, *β* = 82.186(6)°, *γ* = 81.713(6)°, *V* = 925.30(12) Å^3, *Z* = 2, *T* = 110.05(10) K, μ(CuKα) = 0.554 mm^{-1}, *Dcalc* =

1.197 g/cm^3, 5581 reflections measured (9.69° ≤ 2Θ ≤ 134.16°), 3303 unique (R_{int} = 0.0246, R_{sigma} = 0.0400) which were used in all calculations. The final R_1 was 0.0480 (I > 2σ(I)) and wR_2 was 0.1367 (all data).

6.7. Supplemental Single Crystal X-ray Diffraction Data

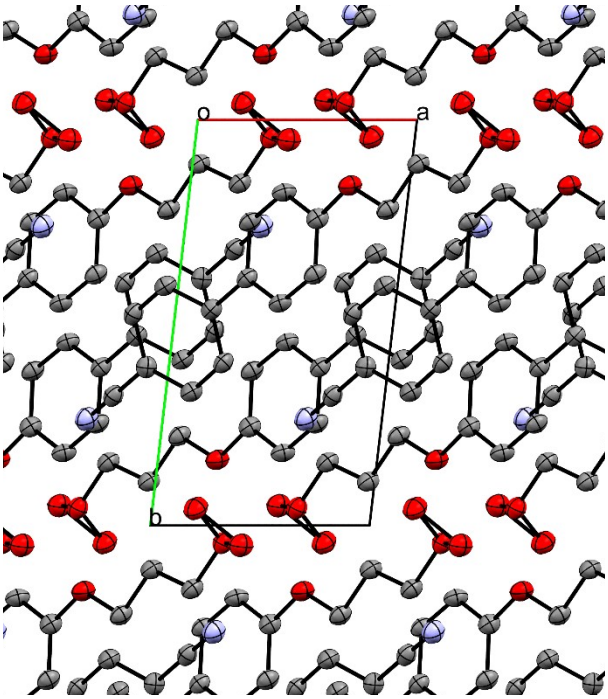

Figure SI-8: Packing in the crystalline state of compound **1** as determined by single crystal XRD (P-1(2) space group). Hydrogen atoms are excluded and the carbon atoms of the cyclopropyl ring are coloured red, both for clarity

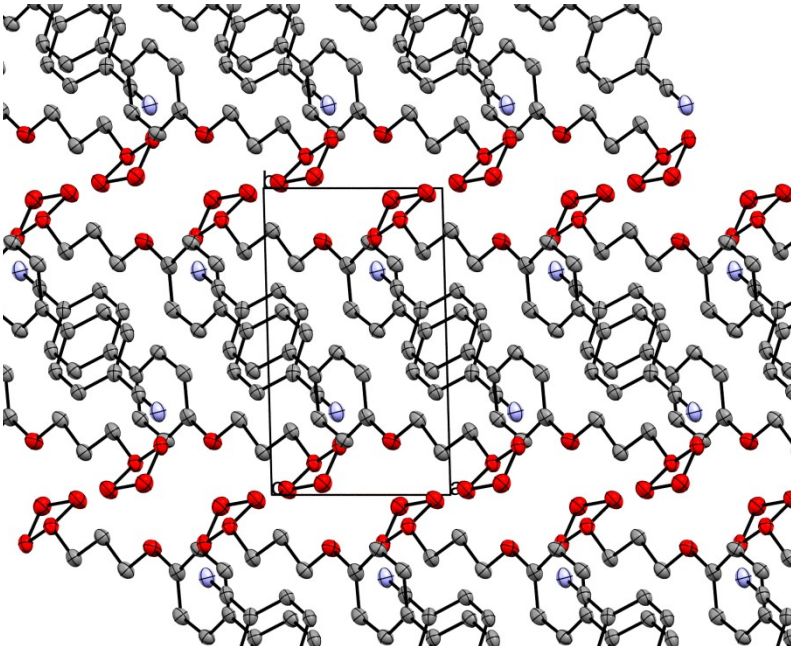

Figure SI-9: Packing in the crystalline state of compound **2** as determined by single crystal XRD (P-1 space group). Hydrogen atoms are excluded and the carbon atoms of the cyclobutyl ring are coloured red, both for clarity

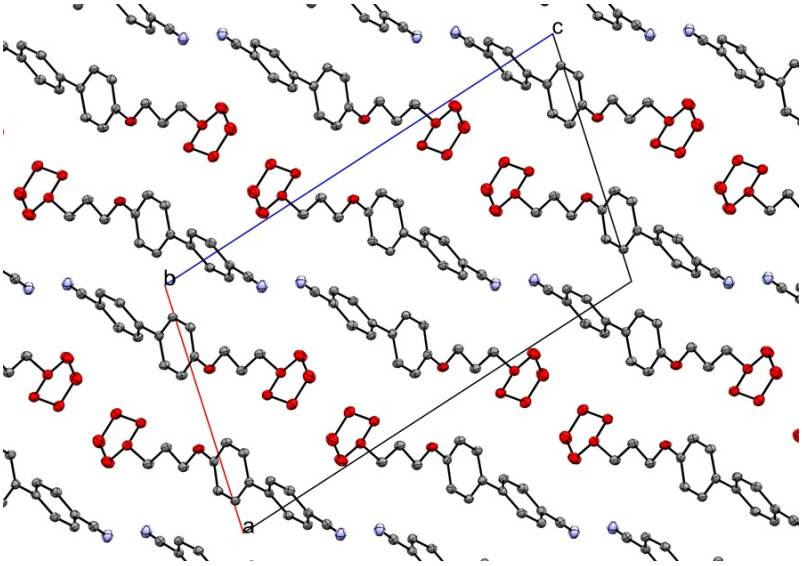

Figure SI-10: Packing in the crystalline state of compound **3** as determined by single crystal XRD (p21/n space group). Hydrogen atoms are excluded and the carbon atoms of the cyclopentyl ring are coloured red, both for clarity

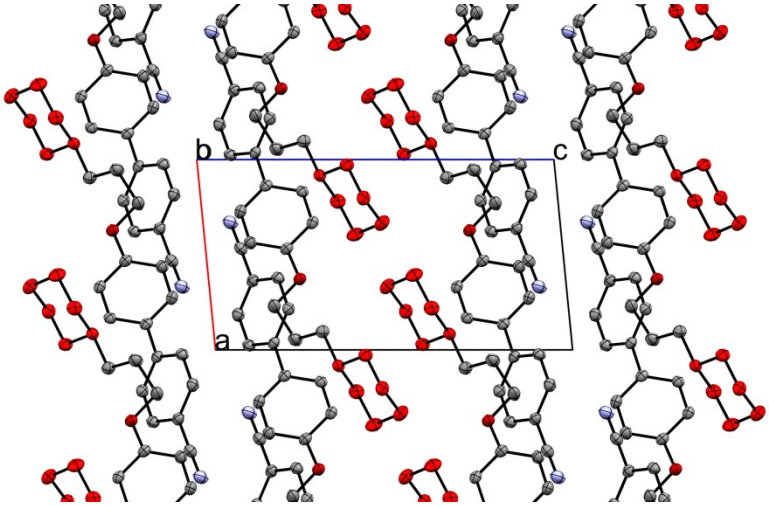

Figure SI-11: Packing in the crystalline state of compound **4** as determined by single crystal XRD ($P\bar{1}$ space group). Hydrogen atoms are excluded and the carbon atoms of the cyclohexyl ring are coloured red, both for clarity

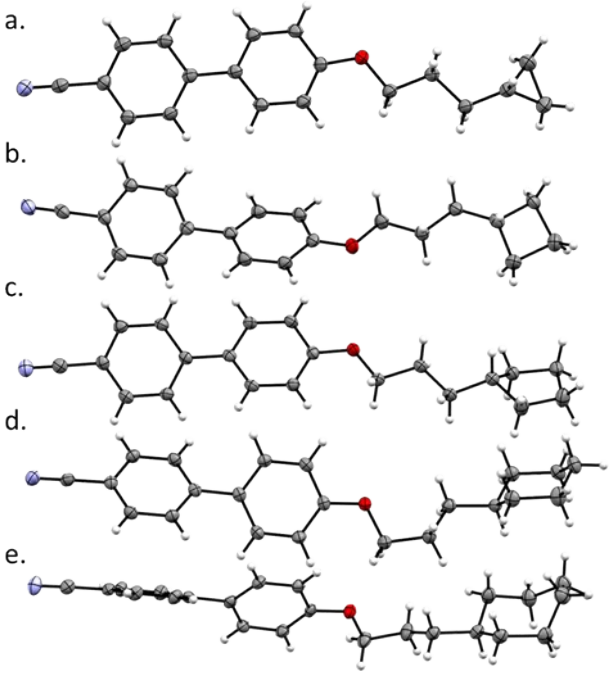

Figure SI-12: Thermal ellipsoid models (50% probability level) of compounds **1** (a, space group P-1), **2** (b, space group P-1) **3** (c, space group $P2_1/n$), **4** (d, space group P-1) and **5** (e, space group P-1) obtained by single crystal XRD.

6.8. Discussion of Single Crystal X-ray Diffraction Data

Cyclopropyl and cyclobutyl rings are effectively rigid, whereas larger rings can adopt a number of conformers [34] with the lowest energy forms being half-boat (**3**), boat (**4**) and twist-boat (**5**) for cyclopentyl, cyclohexyl and cycloheptyl, respectively. To determine the conformation of the terminal rings we grew single crystals of compounds **1** - **5** suitable for structure determination by X-ray diffraction. For compounds **4** and **5** the end-to-end distances in the solid state (**4** = 17.924(2) Å, **5** = 18.329(3) Å) were found to be slightly smaller than those obtained from DFT calculations (**4** = 18.73 Å, **5** = 18.78 Å) due to the presence of a single *gauche* torsion in the spacer (Figure 2b, 2c). For **1** - **3** the spacer was found to be in its all *trans* conformer and so the molecular length (16.941(2), 17.627(3) and 18.140(2) Å respectively) from XRD is comparable to that obtained by DFT calculations (16.99 Å, 17.62 Å and 18.10 Å respectively).

7. References

1. M. S. Lowry, J. I. Goldsmith, J. D. Slinker, R. Rohl, R. A. Pascal, G. G. Malliaras and S. Bernhard, *Chem Mater*, 2005, **17**, 5712-5719.
2. C. P. Johnston, R. T. Smith, S. Allmendinger and D. W. C. MacMillan, *Nature*, 2016, **536**, 322-325.
3. T. Qin, J. Cornella, C. Li, L. R. Malins, J. T. Edwards, S. Kawamura, B. D. Maxwell, M. D. Eastgate and P. S. Baran, *Science*, 2016, **352**, 801-805.
4. R. J. Mandle and J. W. Goodby, *Liq Cryst*, 2017, **44**, 656-665.
5. L. J. Perez, W. L. Ng, P. Marano, K. Brook, B. L. Bassler and M. F. Semmelhack, *J Med Chem*, 2012, **55**, 9669-9681.
6. Y. F. Tian, A. B. Ling, R. Fang, R. X. Tan and Z. Q. Liu, *Green Chem*, 2018, **20**, 3432-3435.
7. M. J. Frisch, G. W. Trucks, H. B. Schlegel, G. E. Scuseria, M. A. Robb, J. R. Cheeseman, G. Scalmani, V. Barone, B. Mennucci, G. A. Petersson, H. Nakatsuji, M. Caricato, X. Li, H. P. Hratchian, A. F. Izmaylov, J. Bloino, G. Zheng, J. L. Sonnenberg, M. Hada, M. Ehara, K. Toyota, R. Fukuda, J. Hasegawa, M. Ishida, T. Nakajima, Y. Honda, O. Kitao, H. Nakai, T. Vreven, J. A. Montgomery Jr., J. E. Peralta, F. Ogliaro, M. J. Bearpark, J. Heyd, E. N. Brothers, K. N. Kudin, V. N. Staroverov, R. Kobayashi, J. Normand, K. Raghavachari, A. P. Rendell, J. C. Burant, S. S. Iyengar, J. Tomasi, M. Cossi, N. Rega, N. J. Millam, M. Klene, J. E. Knox, J. B. Cross, V. Bakken, C. Adamo, J. Jaramillo, R. Gomperts, R. E. Stratmann, O. Yazyev, A. J. Austin, R. Cammi, C. Pomelli, J. W. Ochterski, R. L. Martin, K. Morokuma, V. G. Zakrzewski, G. A. Voth, P. Salvador, J. J. Dannenberg, S. Dapprich, A. D. Daniels, Ö. Farkas, J. B. Foresman, J. V. Ortiz, J. Cioslowski and D. J. Fox, *Gaussian 09 revison E01*, 2009.
8. K. Itoh, M. Kori, Y. Inada, K. Nishikawa, Y. Kawamatsu and H. Sugihara, *Chem Pharm Bull (Tokyo)*, 1986, **34**, 1128-1147.
9. A. D. Becke, *J. Chem. Phys.*, 1993, **98**, 5648-5652.
10. C. T. Lee, W. T. Yang and R. G. Parr, *Phys. Rev. B*, 1988, **37**, 785-789.
11. M. J. Frisch, G. W. Trucks, H. B. Schlegel, G. E. Scuseria, M. A. Robb, J. R. Cheeseman, G. Scalmani, V. Barone, G. A. Petersson, H. Nakatsuji, X. Li, M. Caricato, A. V. Marenich, J. Bloino, B. G. Janesko, R. Gomperts, B. Mennucci, H. P. Hratchian, J. V. Ortiz, A. F. Izmaylov, J. L. Sonnenberg, Williams, F. Ding, F. Lipparini, F. Egidi, J. Goings, B. Peng, A. Petrone, T. Henderson, D. Ranasinghe, V. G. Zakrzewski, J.

Gao, N. Rega, G. Zheng, W. Liang, M. Hada, M. Ehara, K. Toyota, R. Fukuda, J. Hasegawa, M. Ishida, T. Nakajima, Y. Honda, O. Kitao, H. Nakai, T. Vreven, K. Throssell, J. A. Montgomery Jr., J. E. Peralta, F. Ogliaro, M. J. Bearpark, J. J. Heyd, E. N. Brothers, K. N. Kudin, V. N. Staroverov, T. A. Keith, R. Kobayashi, J. Normand, K. Raghavachari, A. P. Rendell, J. C. Burant, S. S. Iyengar, J. Tomasi, M. Cossi, J. M. Millam, M. Klene, C. Adamo, R. Cammi, J. W. Ochterski, R. L. Martin, K. Morokuma, O. Farkas, J. B. Foresman and D. J. Fox, *Gaussian G16 revision A03* , 2016.

12. D.A. Case, I. Y. Ben-Shalom S.R. Brozell, D.S. Cerutti, T.E. Cheatham, III, V.W.D. Cruzeiro, T.A. Darden,; R.E. Duke, D. G., G. Giambasu, T. Giese, M.K. Gilson, H. Gohlke, A.W. Goetz, D. Greene, R Harris,; N. Homeyer, Y. H., S. Izadi, A. Kovalenko, R. Krasny, T. Kurtzman, T.S. Lee, S. LeGrand, P. Li, C. Lin,; J. Liu, T. L., R. Luo, V. Man, D.J. Mermelstein, K.M. Merz, Y. Miao, G. Monard, C. Nguyen, H.; Nguyen, A. O., F. Pan, R. Qi, D.R. Roe, A. Roitberg, C. Sagui, S. Schott-Verdugo, J. Shen, C.L.; Simmerling, J. S., J. Swails, R.C. Walker, J. Wang, H. Wei, L. Wilson, R.M. Wolf, X. Wu, L. Xiao, Y.; Xiong, D. M. Y. a. P. A. K., AMBER 2019. University of California: San Francisco, 2019.
13. C. I. Bayly, P. Cieplak, W. Cornell and P. A. Kollman, *J. Phys. Chem.*, 1993, **97**, 10269-10280.
14. J. Wang, R. M. Wolf, J. W. Caldwell, P. A. Kollman and D. A. Case, *J Comput Chem*, 2004, **25**, 1157-1174.
15. A. W. Sousa da Silva and W. F. Vranken, *BMC Research Notes*, 2012, **5**, 367-367.
16. N. J. Boyd and M. R. Wilson, *Phys Chem Chem Phys*, 2015, **17**, 24851-24865.
17. M. J. Abraham, T. Murtola, R. Schulz, S. Páll, J. C. Smith, B. Hess and E. Lindahl, *SoftwareX*, 2015, **1-2**, 19-25.
18. S. Páll, M. J. Abraham, C. Kutzner, B. Hess and E. Lindahl, in *Solving Software Challenges for Exascale: International Conference on Exascale Applications and Software, EASC 2014, Stockholm, Sweden, April 2-3, 2014, Revised Selected Papers*, eds. S. Markidis and E. Laure, Springer International Publishing, Cham, 2015, DOI: 10.1007/978-3-319-15976-8_1, pp. 3-27.
19. S. Pronk, S. Páll, R. Schulz, P. Larsson, P. Bjelkmar, R. Apostolov, M. R. Shirts, J. C. Smith, P. M. Kasson, D. van der Spoel, B. Hess and E. Lindahl, *Bioinformatics*, 2013, **29**, 845-854.
20. B. Hess, C. Kutzner, D. van der Spoel and E. Lindahl, *J. Chem. Theor. Comput.*, 2008, **4**, 435-447.
21. D. Van der Spoel, E. Lindahl, B. Hess, G. Groenhof, A. E. Mark and H. J. C. Berendsen, *J. Comput. Chem.*, 2005, **26**, 1701-1718.
22. E. Lindahl, B. Hess and D. van der Spoel, *J. Mol. Model.*, 2001, **7**, 306-317.
23. H. J. C. Berendsen, D. Vanderspoel and R. Vandrunen, *Comput. Phys. Commun.*, 1995, **91**, 43-56.
24. B. Hess, H. Bekker, H. J. C. Berendsen and J. G. E. M. Fraaije, *J Comput Chem*, 1997, **18**, 1463-1472.
25. U. Essmann, L. Perera, M. L. Berkowitz, T. Darden, H. Lee and L. G. Pedersen, *J. Chem. Phys.*, 1995, **103**, 8577-8593.
26. G. Bussi, D. Donadio and M. Parrinello, *J. Chem. Phys.*, 2007, **126**, 014101.
27. H. J. C. Berendsen, J. P. M. Postma, W. F. van Gunsteren, A. DiNola and J. R. Haak, *J. Chem. Phys.*, 1984, **81**, 3684-3690.
28. S. Nosé, *Mol Phys*, 1984, **52**, 255-268.
29. W. G. Hoover, *Phys Rev A*, 1985, **31**, 1695-1697.
30. M. Parrinello and A. Rahman, *J Appl Phys*, 1981, **52**, 7182-7190.
31. S. Nosé and M. L. Klein, *Mol Phys*, 1983, **50**, 1055-1076.
32. W. Humphrey, A. Dalke and K. Schulten, *J. Mol. Graph.*, 1996, **14**, 33-38.
33. M. F. Palermo, A. Pizzirusso, L. Muccioli and C. Zannoni, *J. Chem. Phys.*, 2013, **138**, 204901.
34. D. F. Bocian, H. M. Pickett, T. C. Rounds and H. L. Strauss, *J Am Chem Soc*, 1975, **97**, 687-695.

35. CrysAlisPro, Oxford Diffraction Ltd. Version 1.171.34.41

36. Empirical absorption correction using spherical harmonics, implemented in SCALE3 ABSPACK scaling algorithm within CrysAlisPro software, Oxford Diffraction Ltd. Version 1.171.34.40

37. “Olex2” crystallography software, J. Appl. Cryst., 2009, 42, 339–341.

38. SHELXT – Integrated space-group and crystal-structure determination, G. M. Sheldrick, Acta Cryst. 2015, A71, 3-8

39. "SHELXL-97" - program for the Refinement of Crystal Structures, G.M. Sheldrick, Acta Cryst. 2008, A64, 112-122.